# Electronic Band Structure of Tetracene−TCNQ and Perylene−TCNQ Compounds

**I. Shokaryev,[†] A. J. C. Buurma,[†] O. D. Jurchescu,[†] M. A. Uijttewaal,[‡] G. A. de Wijs,[‡] T. T. M. Palstra,[†] and R. A. de Groot*[,†,‡]**

*Solid State Chemistry Laboratory, University of Groningen, Zernike Institute for Advanced Materials, Nijenborgh 4, 9747 AG Groningen, The Netherlands, and Electronic Structure of Materials, University of Nijmegen, Toernooiveld 1, 6525 ED Nijmegen, The Netherlands*

*Received: July 10, 2007; In Final Form: December 15, 2007*

The relationship between the crystal structures, band structures, and electronic properties of acene−TCNQ complexes has been investigated. We focus on the newly synthesized crystals of the charge-transfer salt tetracene−TCNQ and similar to it perylene−TCNQ, potentially interesting for realization of ambipolar transport. The band structures were calculated from first principles using density-functional theory (DFT). Despite the similarity in the crystal structures of the acene−TCNQ complexes studied here, the band structures are very different. Hole and electron transport properties are predicted to be equally good in perylene−TCNQ, in contrast to the tetracene−TCNQ, which has good transport properties for electrons only. The estimated degree of charge transfer for tetracene−TCNQ is 0.13e and for perylene−TCNQ 0.46e.

## 1. Introduction

Organic electronics is a rapidly developing branch of physics, chemistry, and technology. The success of practical applications of organic semiconductors in fabrication of electronic devices such as field effect transistors (FETs)[1,2] and light emitting diodes (LEDs)[3] stimulates further research in this field. For this reason various organic semiconductors were synthesized and studied.[4−6] Organic semiconductors are mostly p-type, leading to prevalent p-type conduction; however, n-type behavior has been realized.[2,7−9] Several n-type organic transistors have been fabricated using TCNQ (tetracyanoquinodimethane) single crystals.[10,11] The combination of both p-type and n-type behavior would enable an ambipolar-FET. This can be used in the elementary units of CMOS logic invertors.[12−14] Various acene−TCNQ compounds such as (antracene,[15] tetracene,[16] perylene[17])−TCNQ known as weak charge-transfer salts, exhibit an alternating stacking sequence of p-type and n-type semiconductor layers of planar $\pi$-conjugated molecules (layered heterostructure). This leads to one-dimensional electrical properties. Single crystals of these materials may be suitable to build ambipolar FETs.[19] Recently, ambipolar behavior was reported in the single-crystal charge-transfer salt (BEDT-TTF)($F_2$TCNQ) by Hasegawa et al.[20] Several conditions must be simultaneously satisfied for a successful ambipolar functioning. First, a properly chosen electrode material with a Fermi level in the middle of the relatively small band gap enables the introduction of both holes and electrons in the material, as the barrier for electron and hole injection is almost equal and low enough for both types of charge carriers. Second, trapping states and various defects deteriorate good conducting properties and, therefore, materials must be sufficiently purified.[2] The third important issue, which plays a crucial role in the discussion of the band-like transport properties, is the electronic structure of the bands where electrons and holes are injected. These are the highest occupied molecular orbital band (HOMO band) and the lowest unoccupied molecular orbital band (LUMO band). The electronic band structure relates to the crystal structure and, therefore, is an intrinsic property that in turn influences measured values of the charge carrier mobility. The basic idea behind synthesizing various acene−TCNQ structures is to satisfy the aforementioned conditions, *i.e.*, to tune the band gap as well as transport properties. This is the main aim of HOMO−LUMO engineering. The simple schematic energy band picture (see Figure 1) shows that by choosing an acene one can get a new compound with smaller band gap and a new HOMO and LUMO bands.

In this paper the electronic band structures of recently synthesized tetracene−TCNQ[16] and similar perylene−TCNQ[17] complexes are studied and compared. Also we correlate the experimental transport properties with calculated electronic band structure.

## 2. Results and Discussions

**2.1. Interpretation of the Band Structure.** Because there are no calculations on the band structure of TCNQ itself, contrary to the cases for tetracene[21] and perylene,[22] we consider it first. The band dispersion of the LUMO band in three main directions X($a$*), Y($b$*), and Z($c$*) is almost isotropic. This result is in full agreement with the observed isotropic mobility in the **ab**-plane as measured in a FET with TCNQ single crystals as the active layer.[11] The lack of anisotropy is remarkable because the interactions in **a** and **b** directions have different origins. In the **b**-direction cyano groups interact with $\pi$-electrons of the phenyl group of the neighboring molecule, whereas in the **a**-direction cyano−cyano interactions are dominant. This follows from the examination of the shortest interatomic distances in the crystal structure. In the **a** direction the cyano−cyano distance ($\cong$3.4 Å) is the shortest while in the **b** direction the cyano−phenyl-group ($\cong$3.5 Å) is the shortest, as shown in Figure 2.

The band structure and the crystal structure of tetracene−TCNQ is shown in Figure 3. The valence band is very narrow in comparison with the conduction band in the direction of the stacking **a**.

* Corresponding author. E-mail: R.deGroot@science.ru.nl.
[†] University of Groningen.
[‡] University of Nijmegen.

10.1021/jp0753777 CCC: $40.75 
Published on Web 02/20/2008

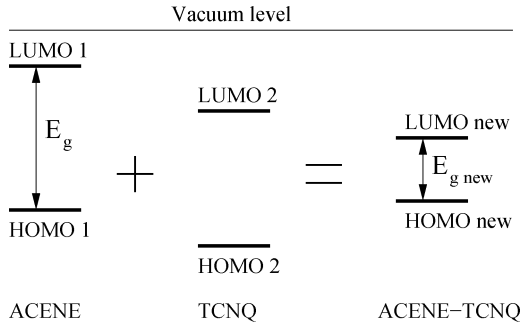


**Figure 1.** HOMO−LUMO engineering. Schematic positions of the acene and TCNQ bands (adapted from ref 30).

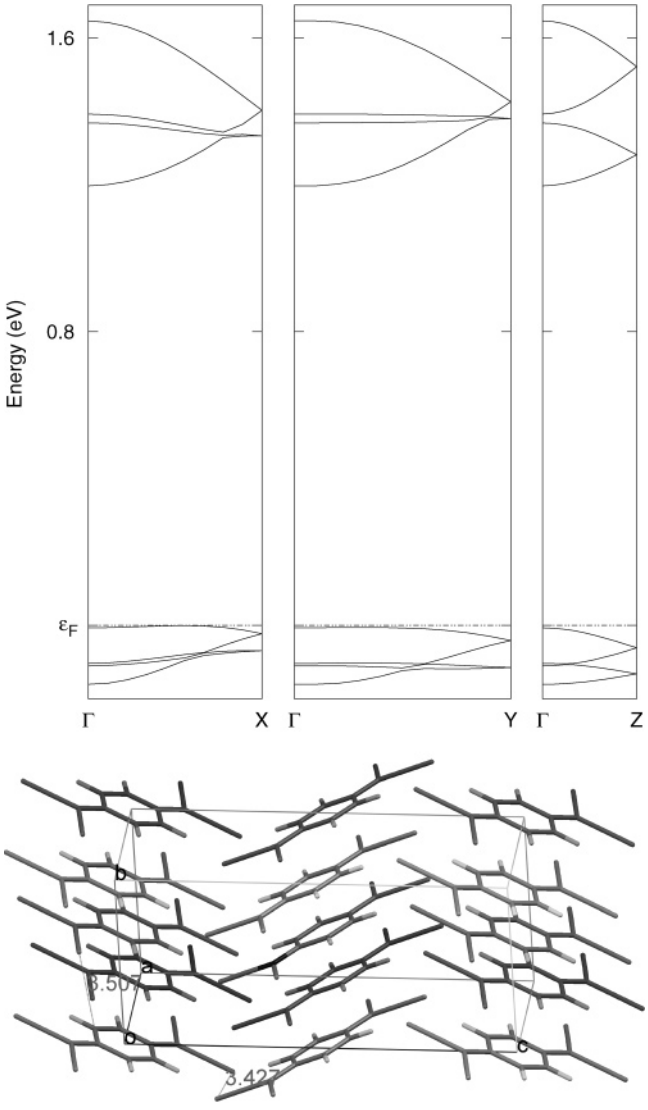


**Figure 2.** Electronic structure of the top of the valence and the bottom of the conduction bands of TCNQ along $X = (\mathbf{a}^*/2, 0, 0)$, $Y = (0, \mathbf{b}^*/2, 0)$, and $Z = (0, 0, \mathbf{c}^*/2)$ direction. $\mathbf{a}^*$, $\mathbf{b}^*$, and $\mathbf{c}^*$ correspond to the directions of **a**, **b**, and **c** crystallographic axess. The Fermi energy was chosen on top of the valence band. The view of the TCNQ crystal packing is given below.

Moreover, there is no intersection of the HOMO with the Fermi energy in the Γ−X direction. In other words, no hole transport in the stacking direction is possible. This does not imply that there is no transport possible at all. There is an intersection along the Y−M direction (parallel to Γ−X). This transport has a component in the stacking direction; however, its dispersion is vanishingly small.

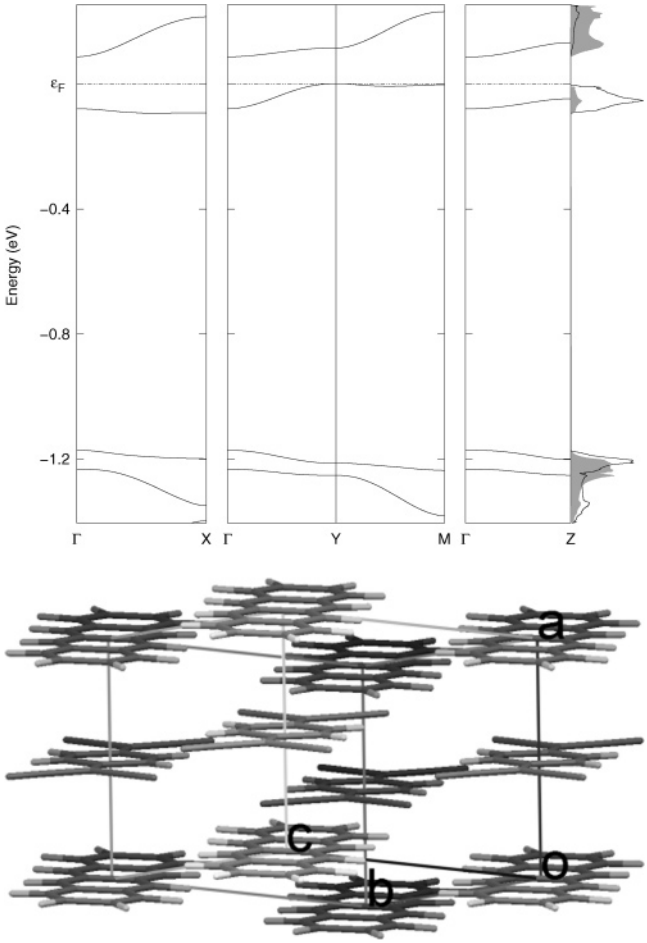


**Figure 3.** Electronic structure of the top of the valence and bottom of the conduction bands of tetracene−TCNQ along $X = (\mathbf{a}^*/2, 0, 0)$, $Y = (0, \mathbf{b}^*/2, 0)$, $M = (\mathbf{a}^*/2, \mathbf{b}^*/2, 0)$, and $Z = (0, 0, \mathbf{c}^*/2)$ direction. The Fermi energy was chosen on top of the valence band. DOS is given in arbitrary units and matched to the band structure. The gray area corresponds to the partial DOS contributed by TCNQ molecule, and the white area corresponds to the tetracene. The view of the tetracene−TCNQ crystal packing is given below. The dissimilarity between HOMO and LUMO dispersions is remarkable.

From the partial density of states (DOS) shown in Figure 3 we found that the conduction band has predominantly TCNQ and the valence band tetracene character. Another and more explicit way to show this is to plot the charge densities of the conduction and the valence bands. The charge density of the conduction band in tetracene−TCNQ crystal is centered mostly at TCNQ molecule (Figure 4a) and has the shape of the LUMO charge density of a single TCNQ molecule as shown in Figure 4b. The valence band charge density is predominantly centered on tetracene and has the shape of the HOMO of a single tetracene molecule. In tetracene−TCNQ the LUMO interacts with HOMO−2 and not with HOMO or HOMO−1 as one can conclude from the band dispersions. This result can be explained qualitatively on the basis of a simple nearest neighbor tight binding model by examining the phase structure of the wave functions of separate tetracene and TCNQ molecules. The difference in the wavefunction nodal structure of the nearest molecules in the stack reflects the bonding-antibonding overlap. To see this, we calculated the charge density distribution of the molecular wave functions of the TCNQ and tetracene molecules separately. The nodal structure of the charge density distributions in Figure 4b shows the alternation of the signs of phase and the shape of the wave function between two regions, separated by a nodal plane. By superimposing these wave functions on

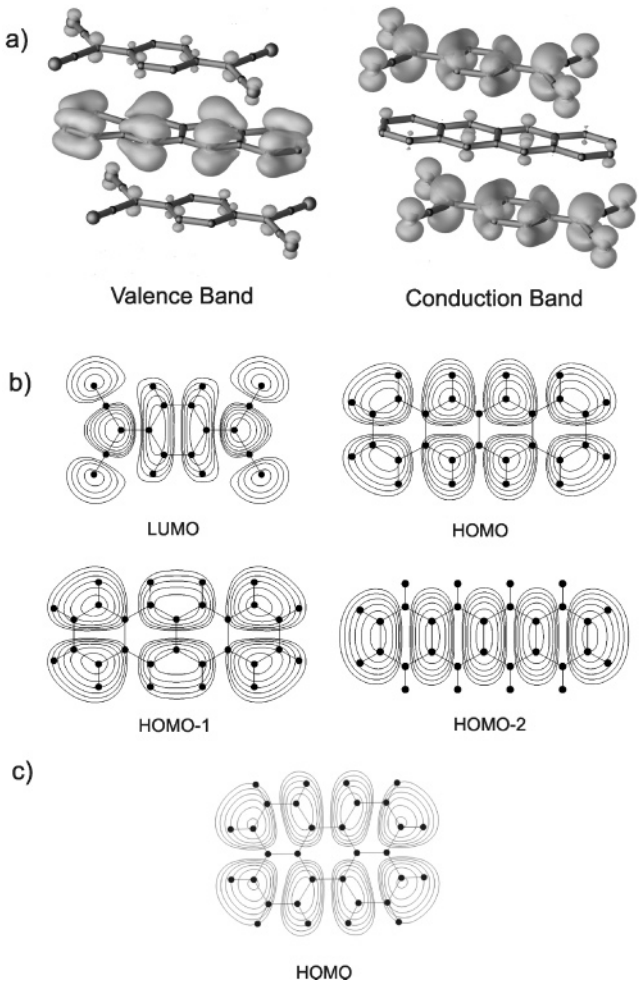


**Figure 4.** (a) Charge density corresponding to the HOMO and the LUMO bands in the bulk of tetracene−TCNQ. Hydrogens are not shown. It is clear that centers of gravity of molecules in the layer are shifted. (b) Plots of the charge density of tetracene and TCNQ molecules at 1.9 Å above the molecular plane, on a logarithmic scale. The difference between the lines corresponds to a difference of a factor $10^{1/4}$ in the electron density. The nodal structure of the LUMO of TCNQ is similar to the HOMO−2 of tetracene but different from HOMO and HOMO−1. (c) Plot of the HOMO charge density of single perylene molecule.

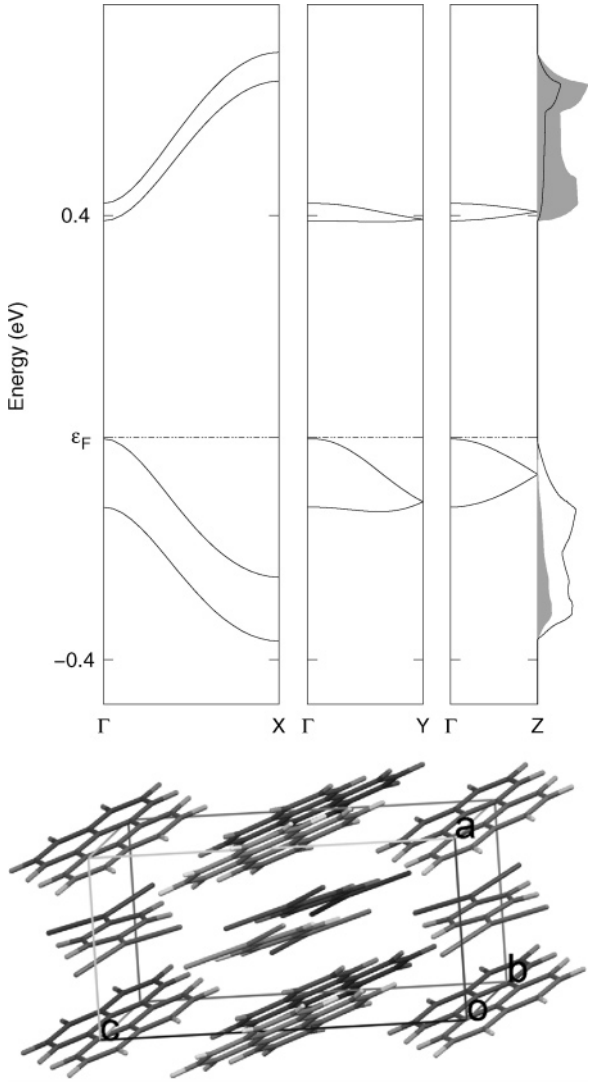


**Figure 5.** Electronic structure of the top of the valence and bottom of the conduction bands of perylene−TCNQ along $X = (\mathbf{a}^*/2, 0, 0)$, $Y = (0, \mathbf{b}^*/2, 0)$, and $Z = (0, 0, \mathbf{c}^*/2)$ direction. The Fermi energy was chosen on top of the valence band. DOS is given in arbitrary units and matched to the band structure. The gray area corresponds to the partial DOS contributed by TCNQ and the white area corresponds to perylene. The view of the perylene−TCNQ crystal packing is given below.

top of each other as if they were in the tetracene−TCNQ crystal we can see how the wave functions overlap in the direction perpendicular to the molecular plane. The HOMO and the HOMO−1 of tetracene have a nodal plane along the long molecular axis but the HOMO−2 and the LUMO of TCNQ do not, as displayed in Figure 4b. Hence upon the superimposing of TCNQ and tetracene, the resulting overlap between HOMO, HOMO−1 of tetracene and the LUMO of TCNQ is obviously zero, which leads to nondispersive shape of the HOMO and the HOMO−1 bands. On the contrary, the nodal structure of the HOMO−2 wave function of tetracene leads to nonzero overlap with the LUMO of the TCNQ. This results in the dispersive shape of the HOMO−2 and LUMO bands. Note that nonzero overlap of TCNQ LUMO and tetracene HOMO−2 here is a direct consequence of the finite angle between stacking direction and the normal of the molecular planes. Because of this, the central maximum of the tetracene HOMO−2 is not directly above the central nodal plane (separating the left and right halves) of the TCNQ LUMO. Instead, it is shifted toward one of the two banana-shaped maxima of the TCNQ LUMO, so that a nonzero overlap exists. The striking difference of TCNQ LUMO and tetracene HOMO−2 also explains why the LUMO−HOMO−2 gap increases going from Γ to X in the Brillouin zone (BZ); *i.e.* that within the tight-binding picture the interaction between both molecular orbitals is essentially nonbonding at Γ whereas the bonding and antibonding interactions are most effective at X.

It is interesting to compare the band structure of tetracene−TCNQ with the band structure of compound perylene−TCNQ, because of their similar crystal structure and availability of electrical measurements. The band structure of perylene−TCNQ is given in the Figure 5 with the corresponding crystal packing. The valence and conduction bands of perylene−TCNQ appear in pairs because the unit cell contains two perylene and two TCNQ molecules. The valence and the conduction bands of tetracene−TCNQ differ from that of perylene−TCNQ. Although the distance between the acene and the TCNQ molecules in the stack of the tetracene−TCNQ compound is similar to that in perylene−TCNQ, the conduction bandwidths are completely different. It should be stressed that not only the intermolecular distance determines the magnitude of $p_z-p_z$ orbital overlap but

**TABLE 1: DFT Band Gaps and Band Widths (eV)[a]**

| compound (pristine) | DFT band gap | direction | HOMO band | LUMO band | effective mass $m^*_e m_0$ | effective mass $m^*_h m_0$ |
|---|---|---|---|---|---|---|
| TCNQ | 1.20 | X | 0.016 | 0.136 | 1.88 | |
| | | Y | 0.034 | 0.183 | 2.34 | |
| | | Z | 0.054 | 0.084 | | |
| perylene−TCNQ | 0.39 | X | 0.249 | 0.251 | 0.94 | 0.91 |
| (perylene) | (1.56) | | | | | |
| | | Y | 0.113 | 0.002 | | |
| | | Z | 0.064 | 0.016 | | |
| tetracene−TCNQ | 0.08 | X | 0.014 | 0.128 | 1.97 | |
| (tetracene)[21] | (1.23) | | | | | |
| | | Y | 0.080 | 0.030 | | |
| | | Z | 0.052 | 0.045 | | |

[a] The effective mass is given for the most dispersive bands. The band gap for pristine perylene was estimated from calculation of the ground state of the single perylene molecule as the HOMO−LUMO distance.

also the relative position of the molecules in the plane parallel to the molecular planes, which defines the area of the overlap and the relative positions of the positive and negative phases of the wave functions. In contrast to the crystal structure of the tetracene−TCNQ, the perylene and the TCNQ molecules are shifted sidewise (Figure 5) with respect to each other (along the short molecular axis of the perylene viewed perpendicular to its molecular plane), leading to a nonzero overlap between the LUMO of the TCNQ and the HOMO of the perylene wave functions (see Figure 4b,c). With a similar reasoning as for tetracene−TCNQ above, here the sidewise shift and the different shape of TCNQ LUMO and perylene HOMO explain why the HOMO−LUMO interactions are maximal at the BZ edge. The above analysis shows that the nodal structure of the wave functions of the molecules comprising the molecular crystal and their relative orientation within a crystal alone contain already vital information on the HOMO and the LUMO interaction.

The total band widths and the direct band-gaps following from the calculated band structure are summarized in Table 1. Despite the common deficiency of DFT to estimate the value of the band gap (typically the band gap is 50−80% underestimated),[23] it is still possible to compare the general trends of going from one acene−TCNQ complex to another. This is in agreement with the schematic band diagram shown in Figure 1. Acene−TCNQs have smaller band gap than TCNQ itself and their pristine compounds. The effective electron ($m^*_e$) and hole masses ($m^*_h$) of charge carriers for the most dispersive bands are also given in the Table 1. They were obtained from the band structure by fitting

$$\frac{1}{m^*} = \frac{1}{\hbar^2}\frac{\mathrm{d}^2 E(\mathbf{k})}{\mathrm{d}\mathbf{k}^2} \qquad (1)$$

at the top of the valence and conduction bands in terms of electron rest mass $m_0$. The effective electron mass of charge carriers in perylene−TCNQ is 2 times smaller than in TCNQ, promising higher mobilities because mobility is inversely proportional to the effective mass. Moreover holes have also almost the same effective mass as electrons, suggesting that perylene−TCNQ can be used for hole transport as well. This is a very interesting result because the symmetry between electron and hole conduction point to the usefulness of perylene−TCNQ for ambipolar FETs. Tetracene−TCNQ shows no improvement because the effective electron mass in the staking direction is nearly the same as in TCNQ and flatness of the valence band makes injected holes extremely heavy, which precludes tetracene−TCNQ from hole conduction and thus from ambipolar transport.

**TABLE 2: Calculated Bond Lengths (Å) of TCNQ[a]**

| bond | CT | TCNQ | $TCNQ^-$ |
|---|---|---|---|
| C1−C2 | 1.432 | 1.439 | 1.424 |
| C1−C4 | 1.405 | 1.400 | 1.434 |
| C2−C3 | 1.362 | 1.361 | 1.377 |
| C4−C5 | 1.415 | 1.420 | 1.410 |
| N1−C5 | 1.169 | 1.168 | 1.174 |

[a] CT refers to the charge-transfer crystal. TCNQ and $TCNQ^-$ stay for single neutral and charged molecules.

**2.2. Estimation of the Charge Transfer.** Acene−TCNQ complexes belong to the class of materials called charge-transfer salts.[24] TCNQ acts as an acceptor due to its high electron affinity, attracting electrons from the acene. This leads to the charge redistribution in the unit cell, which can be described as the partial electron charge transfer from the acene to the TCNQ. We inferred the partial charge transfer from the HOMO of the tetracene to the LUMO of the TCNQ by analyzing the bond lengths and the total charge distribution in the unit cell in the way it was done in the work of Brocks.[25] We calculated the ground state geometry of neutral TCNQ and $TCNQ^-$. The bond lengths are listed in Table 2 (the bonds are labeled as in Figure 6). We interpret differences in the bond lengths in terms of charge transfer. The bond lengths, found from the geometry of TCNQ in the optimized tetracene−TCNQ crystal structure, are always between the neutral and charged case indicating a partial charge transfer. Note that the changes in charge density are not reflected in the N1−C5 and C2−C3 bond lengths (because they barely change) because of the nodal planes in the LUMO (see Figure 4b). The same is valid for tetracene. The charge transfer was calculated to be 0.1e, using empirical relations between the bond lengths and the electronic charge in our previous

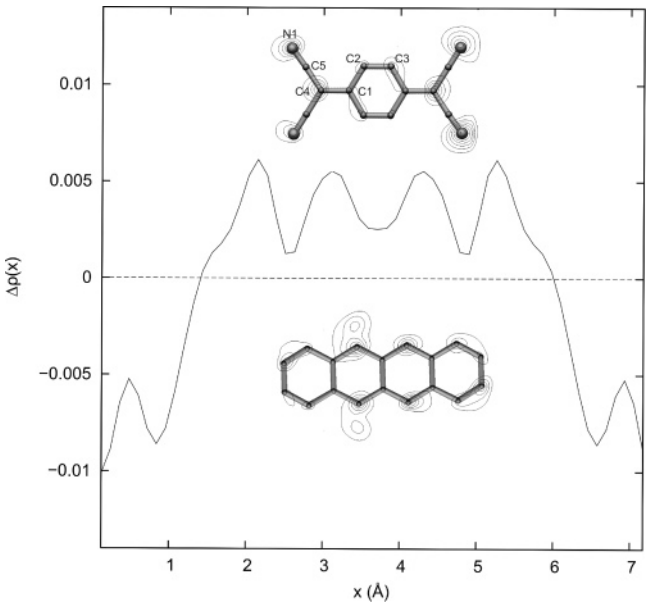


**Figure 6.** Charge density along the stacking direction $\Delta\rho(x) = \int\int(\rho_{A+B}(\mathbf{r}) - \rho_A(\mathbf{r}) - \rho_B(\mathbf{r}))\,\mathrm{d}y\,\mathrm{d}z$. The area of the integration is the crosscut of the unit cell by a plane perpendicular to the **a**-axis. The curve shows the accumulation of the charge on TCNQ site and the depletion on the tetracene, indicating the charge transfer. The amount of the charge transfer is the area under the upper part of the curve. The insets to the figure correspond to the contour plots of the positive (centered mostly at TCNQ) and the negative (centered mostly at tetracene) values of $\rho(\mathbf{r})$ at the level of 0.7 Å above the molecular plane.

work.[16] In this article we estimate the partial charge transfer directly by examining the charge density given by DFT explicitly. We calculated the following charge density distribution: $\Delta\rho(\mathbf{r}) = \rho_{A+B}(\mathbf{r}) - \rho_A(\mathbf{r}) - \rho_B(\mathbf{r})$, where $\rho_{A+B}(\mathbf{r})$ is the charge density in the unit cell of tetracene−TCNQ and $\rho_A(\mathbf{r})$, $\rho_B(\mathbf{r})$ are the tetracene and the TCNQ molecular charge densities within the same geometry. The positive part of $\Delta\rho(\mathbf{r})$ shows the accumulation and the negative part the depletion of the electronic charge. In the Figure 6 we plotted $\Delta\rho(\mathbf{r})$ in the stacking direction. The insets of the Figure 6 show that the charge accumulation pattern at the TCNQ is similar to the shape of the LUMO of the neutral TCNQ molecule and the charge depletion pattern on tetracene looks like the HOMO of the neutral tetracene. From Figure 6 we estimated the charge transfer to be 0.13*e*. For perylene−TCNQ the charge transfer is estimated to be 0.46e, suggesting better orbital overlap and thus better conductive properties than in tetracene−TCNQ. A quantitative, unique definition of charge transfer is difficult to give, however.

**2.3. Discussions of Experimental Results.** The measurements on devices in FET geometry for tetracene−TCNQ were complicated by the lack of adhesion of the crystal to the gate dielectric, the presence of possible traps and injection barriers.[26] Therefore, no experimental results have yet been reported. However, on the basis of the calculated band structure, we can state that this material is not suitable for ambipolar transport as was presumed before.[26]

In general, several conditions must be satisfied to realize ambipolar transport. We mentioned already the electrode material and the influence of defect states in the introduction. Another consideration is the effect of temperature. The interaction of electrons (holes) with the crystal lattice plays a role in transport mechanism in organic semiconductors with the increase of temperature.[27] This leads to the decrease of the HOMO and the LUMO bandwidths evolving from band-like to hopping-like transport. The solution of the Holstein−Peierls model, describing coupling of charge carriers with the phonons, has been successfully applied by Hannewald et al.[28,29] to several organic molecular crystals, where the *ab initio* DFT results were involved as an important ingredient. However, the calculated DFT results indicate that hole transport is impossible even at low temperature in the case of tetracene−TCNQ.

The experimental results on perylene−TCNQ were more successful. The measurements on FETs fabricated from perylene−TCNQ showed the electron mobility as high as 0.3 $cm^2/(V\ s)$.[30] The band structure suggests that *hole* transport with similar mobility is also possible in perylene−TCNQ because the valence and conduction bands are almost equally dispersive. In practice it is more complicated to realize because deep and shallow trap states are present. They alter the mobility significantly. Notice that the electron mobility (1.6 $cm^2/(V\ s)$)[11] measured in TCNQ is several times higher than obtained from the measurements in perylene−TCNQ. However, the calculated effective mass corresponding to conduction bandwidth of perylene−TCNQ is 2 times smaller than in TCNQ (see Table 1 for details), indicating that in principle the mobility measured in perylene−TCNQ can be even higher than in TCNQ both for holes and for electrons, assuming a comparable influence of phonons.

Bandwidths and gaps are summarized in Table 1. The decrease in the band gap compared to pure TCNQ is clear. This decrease in the band gap, as mentioned previously, is advantageous for ambipolar FET behavior however it should not be too small.

## 3. Conclusions

The band structures of tetracene−TCNQ and perylene−TCNQ complexes were calculated to get a better insight into their transport properties. It complements experimental evidence, which, due to a number of experimental conditions, provides us not always with consistent results. The electron mobility measured in perylene−TCNQ is 0.3 $cm^2/(V\ s)$. Intrinsically, perylene−TCNQ crystals are better for electron conduction than TCNQ crystals, as follows from the band structure; however, the highest electron mobility measured in TCNQ was 1.6 $cm^2/(V\ s)$. Thus even higher electron mobilities in perylene−TCNQ are expected under equal experimental conditions. The *hole* mobility in perylene−TCNQ has not been measured. However, conduction and valence bands are equally wide and dispersive, implying equal mobilities both for *holes* and for electrons. This makes perylene−TCNQ an interesting material for possible application in ambipolar FETs.

We were not able to determine either electron or *hole* mobilities for tetracene−TCNQ. The electronic band structure shows that the electron mobility in tetracene−TCNQ should be lower than in perylene−TCNQ and *holes* are expected to be immobile. The estimated value of the charge transfer for tetracene−TCNQ is 0.13e and for perylene−TCNQ is 0.46e.

Organic semiconductors suitable for the ambipolar transport should have the following properties: a relatively small band gap that reduces the injection barriers both for holes and for electrons and highly dispersive valence and conduction bands that give low bare effective mass to the charge carriers. For ambipolar transport the perylene−TCNQ compound turns out to be more promising. Tetracene−TCNQ with a similar crystal structure is orders of magnitude worse. The differences reflect the different symmetries of the HOMO and LUMO states involved.

**Acknowledgment.** This work work was supported by the NWO breedte strategie program MSC*plus* and is part of the research programme of the Stichting voor Fundamenteel Onderzoek der Materie (FOM) with financial support from the Nederlandse Organisatie voor Wetenschappelijk Onderzoek (NWO). We acknowledge R. Zeis and C. Kloc for stimulating discussions and for permission to reproduce Figure 1.

## 4. Appendix. Method of Calculation

The electronic band structure calculations represented in this article were performed using an *ab initio* technique based on density-functional theory (DFT)[31] in the generalized gradient approximation (GGA) PW91.[32] This method is implemented in the Vienna *ab initio* Simulation Package (VASP).[33−37] The crystal structures were taken from the literature.[16−18] The present approach was successfully applied to a number of organic semiconductors in particular for pentacene.[21,38−40]

Because X-ray diffraction cannot determine hydrogen positions accurately, for each of the bulk calculations the positions of the atoms in the unit cell were relaxed (while the shape and the volume of the unit cell were kept fixed) using a conjugate gradient algorithm and a tolerance of 10 meV/Å on interatomic forces. For Brillouin zone (BZ) integration we used a Monkhorst−Pack *k*-point mesh[41] with $6 \times 6 \times 6$ points. The energy cutoff on the plane-wave basis set used in all calculations was 400 eV. The charge-density plots for separate molecules were obtained with the same package. For these calculations we used a cubic supercell of $20 \times 20 \times 20$ $Å^3$, which ensures that the periodic molecular replicas do not interact.

## References and Notes

(1) Horowitz, G. *Adv. Mater.* **1998**, *10*, 365.
(2) Dimitrokopouls, C. D.; Malenfant, P. R. L. *Adv. Mater.* **2002**, *14*, 99.
(3) Greenham, N. C.; Moratti, S. C.; Bradley, D. D. C.; Friend, R. H.; Holmes, A. B. *Nature* **1993**, *365*, 628.
(4) Reese, C.; Bao, Z. *J. Mater. Chem.* **2006**, *16*, 329.
(5) Brédas, J. L.; Calbert, J. P.; da Silva Filho, D. A.; Cornil, J. *Proc. Natl. Acad. Sci.* **2002**, *99*, 5804.
(6) Shaw, J. M.; Seider, P. F. *IBM J. Res. Dev.* **2001**, *45*, 3.
(7) Chua, L.-L.; Zaumseil, J.; Chang, J.-F.; Ou, E. C.-W.; Ho, P. K.-H.; Sirringhaus, H.; Friend, R. H. *Nature* **2005**, *434*, 194.
(8) Babel, A; Jenekhe, S. A. *J. Am. Chem. Soc.* **2003**, *125*, 13656.
(9) Katz, H. E.; Lovinger, A. J.; Johnson, J.; Kloc, C.; Siegrist, T.; Li, W.; Lin, Y.-Y.; Dodabalapur, A. *Nature* **2000**, *404*, 478.
(10) Brown, A. R.; de Leeuw, D. M.; Lous, E. J.; Havinga, E. E. *Synth. Met.* **1994**, *66*, 257.
(11) Menard, E.; Podzorov, V.; Hur, S.-H.; Gaur, A.; Gershenson, M. E.; Rogers, J. A. *Adv. Mater.* **2004**, *16*, 2097.
(12) Meijer, E. J.; Leeuw, D. M.; Setayesh, S.; Van Veenendaal, E.; Huisman, B.-H.; Blom, P. W. M.; Hummelen, J. C.; Scherf, U.; Klapwijk, T. M. *Nat. Mater.* **2003**, *2*, 678.
(13) Crone, B; Dodabalapur, A.; Lin, Y.-Y.; Filas, R. W.; Bao, Z.; LaDuca, A.; Sarpeshkar, R.; Katz, H. E.; Li, W. *Nature* **2000**, *403*, 521.
(14) Lin, Y.-Y.; Dodabalapur, A.; Sarpeshkar, R.; Bao, Z.; Li, W.; Baldwin, K.; Raju, V. R.; Katz, H. E. *Appl. Phys. Lett.* **1999**, *74*, 2714.
(15) Williams, R. S.; Wallwork, S. C. *Acta Crystallogr. B* **1968**, *24*, 168.
(16) Buurma, A. J. C.; Jurchescu, O. D.; Shokaryev, I.; Baas, J.; Meetsma, A.; de Wijs, G. A.; de Groot, R. A.; Palstra, T. T. M. *J. Phys. Chem. C* **2007**, *111*, 3486.
(17) Tickle, I. J.; Prout, C. K. *J. Chem. Soc., Perkin Trans.* **1973**, *2*, 720.
(18) Long, R. E.; Sparks, R. A.; Trueblood, K. N. *Acta Crystallogr.* **1965**, *18*, 932.
(19) Dodabalapur, A.; Katz, H. E.; Torsi, L.; Haddon, R. C. *Appl. Phys. Lett.* **1995**, *68*, 1108.
(20) Hasegawa, T.; Mattenberger, K.; Takeya, J.; Batlogg, B. *Phys. Rev. B* **2004**, *69*, 245115.
(21) Hummer, K.; Ambrosch-Draxl, C. *Phys. Rev. B* **2005**, *72*, 205205.
(22) Kang, S. J.; Cho, Yi, Y., K, Yoo, K.-H, Whang, C. N. *Synth. Met.* **2005**, *151*, 120.
(23) Godby, R. W.; Schlüter, M.; Sham, L. J. *Phys. Rev. Lett.* **1986**, *56*, 2415.
(24) Jérome, D. *Chem. Rev.* **2004**, *104*, 5565.
(25) Brocks, G. *Phys. Rev. B* **1997**, *55*, 6816.
(26) Buurma, A. J. C. Master thesis (unpublished), 2006.
(27) Coropceanu, V.; Cornil, J.; da Silva, Filho, D. A.; Olivier, Y.; Silbey, R.; Bredas, J. *Chem. Rev.* **2007**, *107*, 926.
(28) Hannewald, K.; Stojanovic, V. M.; Schellekens, J. M. T.; Bobbert, P. A. *Phys. Rev. B* **2004**, *69*, 075211.
(29) Hannewald, K.; Bobbert, P. A. *Appl. Phys. Lett.* **2004**, *85*, 1535.
(30) Zeis, R. Ph.D. thesis, University of Konstanz, 2005.
(31) Kohn, W. *Rev. Mod. Phys.* **1999**, *71*, 1253.
(32) Perdew, J. P.; Chevary, J. A.; Vosko, S. H.; Jackson, K. A.; Pederson, M. R.; Singh, D. J.; Fiolhais, C. *Phys. Rev. B* **1992**, *46*, 6671.
(33) Kresse, G.; Hafner, J. *Phys. Rev. B* **1994**, *49*, 14251.
(34) Kresse, G.; Furthmüller, J. *Phys. Rev. B* **1996**, *54*, 11169.
(35) Kresse, G.; Furthmüller, J. *Comput. Mater. Sci.* **1996**, *6*, 15.
(36) Blöchl, P. E. *Phys Rev. B* **1994**, *50*, 17953.
(37) Kresse, G; Joubert, D. *Phys. Rev. B* **1998**, *59*, 1758.
(38) Mattheus, C. C.; de Wijs, G. A.; de Groot, R. A.; Palstra, T. T. M. *J. Am. Chem. Soc.* **2003**, *125*, 6323.
(39) de Wijs, G. A.; Mattheus, C. C.;de Groot, R. A.; Palstra, T. T. M. *Synth. Met.* **2003**, *139*, 109.
(40) Troisi, A.; Orlandi, G. *J. Phys. Chem. B* **2005**, *109*, 1849.
(41) Monkhorst, H. J.; Pack, J. D. *Phys. Rev. B* **1976**, *13*, 5188.